■Ngày nhận bài: 14/3/2022 ■Ngày sửa bài: 22/4/2022 ■Ngày chấp nhận đăng: 09/5/2022

Experimental Strain Responses of Post-tensioning Tendon Anchorage Subjected to Prestressing Force Loss

Thực nghiệm ứng xử biến dạng của vùng neo cáp dự ứng lực căng sau dưới tác dụng mất mát lực dự ứng lực

> PHAN NGOC TUONG VY, DANG NGOC LOI
Urban Infrastructure Faculty, Mien Tay Construction University
Email: dangngocloi@mtu.edu.vn, Tel: +84 912-990-967

ABSTRACT

Prestress force is a key component of prestressed concrete structures. Early detection of prestressing force loss is necessary to ensure structural integrity and minimize long-term maintenance costs. This study presents an experimental investigation of strain responses in post-tensioning tendon anchorage subjected to prestressing force loss. To achieve the objective, first, a post-tensioning anchorage system is equipped with arrays of ESGs (electrical strain gages) for measuring strain responses. The anchorage system is installed on the stressing system, which is used to resist prestress force from the anchorage. Second, strain responses of ESGs arrays are measured under series prestress loss cases. Third, strain variations are utilized to determine stress components sensitive to prestress force loss. Last, empirical equations for prestress loss estimation is proposed based on experimental strain data. The result shows that strain responses in the anchorage are promising to be used for monitoring the health conditions of the anchorage system.

Keywords: Strain response; prestress loss; post-tensioning structure; damage detection.

TÓM TẮT:

Lực dự ứng lực là một thành phần rất quan trọng trong các kết cấu bê tông dự ứng lực. Việc chẩn đoán sớm mất mát lực dự ứng lực là cần thiết nhằm đảm bảo tính toàn vẹn của kết cấu và giảm thiểu chi phí duy tu kết cấu trong thời gian vận hành. Bài viết trình bày nghiên cứu thực nghiệm về ứng xử của biến dạng trong vùng neo cáp dự ứng lực căng sau dưới tác dụng của mất mát dự ứng lực. Để đạt được mục tiêu đề ra, đầu tiên, vùng neo cáp dự ứng lực được lắp đặt với các nhóm cảm biến đo biến dạng để đo ứng xử biến dạng của vùng neo. Hai là, biến dạng từ các nhóm cảm biến đo biến dạng được ghi nhận dưới các trường hợp mất lực dự ứng lực. Ba là, tín hiệu biến dạng từ thực nghiệm được phân tích để xác định các thành phần biến dạng nhạy với sự thay đổi lực căng cáp. Sau cùng, dựa vào dữ liệu biến dạng, các phương trình thực nghiệm được đề xuất để xác định mất lực dự ứng lực trong vùng neo. Kết quả nghiên cứu chỉ ra rằng tín hiệu biến dạng của vùng neo rất tiềm năng để áp dụng cho việc quan trắc sức khỏe vùng neo cáp dự ứng lực căng sau.)

Từ khóa: Biến dạng; mất mát dự ứng lực; kết cấu dự ứng lực căng sau; chẩn đoán hư hỏng

1. INTRODUCTION

The post-tensioning technique has been widely used for the construction of bridges, buildings, and nuclear containment structures. In the technique, prestressing strands are passed through the ducts and anchored into anchorage systems. For post-tensioning concrete structures, prestress force is a key parameter that can reveal the structural health conditions. After the procedure of post-tensioning construction, anchorage zones are prone to instantaneous prestress losses, and time-dependent prestress losses [1].

In recent years, a number of tendon-anchorage failures in post-tensioning bridges in the US have been reported [2, 3]. Even for a newly built post-tensioned PSC girder, the prestress loss could reach up to 7.7% in seven years [4]. When the loss of prestress force reaches a threshold, tensile stress would lead to cracks and/or excessive deflections in

concrete components. Due to its critical role, the prestress force should be properly monitored to ensure structural integrity and to avoid catastrophic structural failures (e.g., the collapse of Genoa Bridge in 2018 [5]).

Various structural health-monitoring techniques have been developed for prestressed concrete members. Visual inspection is the common monitoring technique for tendon anchorage without utilizing any specialized instrumentations. It is applicable when degradation can be visible itself. Vibration-based methods have been developed to identify prestress force [6, 7] by utilizing the vibration properties of a structure, such as natural frequencies. The methods utilize low-order modal parameters, which are insensitive to local and incipient structural damages [8, 9]. Impedance-based methods have been adopted to detect the prestress-loss in post-tensioned concrete structures [10, 11]. Electromechanical impedance responses of a target structure are acquired from low-cost lead-zirconate-titanate patches, and impedance variations are quantified to utilize as a damage indicator. The impedance-based methods have been extensively studied for the health monitoring of various civil structures, including cracks in concrete [12], and delamination of composite structures [13, 14]. However, the impedance features are quite sensitive to changes in environmental conditions [15].

Strain-based methods are regarded as simple and accurate techniques to directly estimate the prestress level by using a well-defined stress-strain relationship (i.e., Hooke's law). To measure strain, electrical strain gages [16], and fiber optic sensors [17] are commonly used. Lan *et al.* [17] embedded an optical fiber with distributed Fiber Bragg Grating into a center wire of a 7-wire strand to estimate stress changes. However, it is found that the installation of the optical fiber in the center wire is extremely difficult. Abdullah *et al.* [16] affixed an array of electrical strain gauges on a multi-strand anchor's faces to detect wire breaks using measured strain variation induced by cutting wires. However, prestress loss induced by cutting wires rarely occurs during operation processes of structures, and cutting wire events causes s changes in measuring signals.

Partial prestress loss of steel strands that causes relatively small strain changes has not been studied so far [10, ludden6]. Thus, it requires determining a strain-stress component, which is the most sensitive to prestress loss to detect early damage strands in anchorage structures. In this study, strain responses of post-tensioning tendon anchorage subjected to prestressing force loss are experimentally assessed. To achieve the objective, first, a post-tensioning anchorage system is equipped with arrays of ESGs for measuring strain responses. The anchorage system is installed on the stressing system, which is used to introduce and resist prestress force from the anchorage. Second, strain responses of ESGs arrays are measured under the losses of the outer and center strands. Third, strain variations are utilized to determine stress components sensitive to prestress force losses. Last, empirical equations for prestress loss estimation is proposed based on experimental strain data.

2. EXPERIMENTAL TEST ON POSTTENSIONING TENDON ANCHORAGE FOR MEASURING STRAIN RESPONSES

2.1 Description of tested structure

A supporting frame made of steel (minimum capacity of 300 tons) was designed to resist the force of prestressing strands, as shown in Figure 1a. The structural frame includes two thick steel-plates connected using four steel tubes. On a dead-end (i.e., the left steel plate), prestressing strands passing were gripped using wedges on an anchor head. On a live end (i.e., the right plate), the strands were passed through into holes, and nine load cells were used to get real applied forces in the nine strands.

A 9-strands anchorage (type E anchorage of VLS post-tensioning system) was installed at the dead end. The bearing plate (27 × 27 × 4.5 cm) and an anchor head (ϕ15.9 cm and H= 70 cm), and the wedges and main components of the anchorage system. The 7-wires prestressing strands (15.2 mm in diameter) were made of Grade 270 (low relaxation steel). The strands had a tensile strength of 260 kN. The left ends of the strands were gripped in the anchor head. The right ends were designed to connect to the jacking system for controlling force.

2.2 Deployment of sensors for measuring strain responses

For the unboned anchorage system, as the anchor head directly anchors prestressing strands, prestress loss in steel strands causes vary mainly in the anchor head rather than the bearing plate [10]. Moreover, the circumferential face of the anchor head refers to attaching sensors.

To capture strain responses of the tested structure, ESGs (F series TML FLA-5-11-1L) were installed on the anchor head, as shown in Figures 1-2. The ESGs were installed in axial and circumferential directions of the anchor head (see Figure 1b-c). Specifically, for the near-top anchor head, six ESGs, called CT1-3 and CT6-8, were positioned at the near-top anchor head (3 mm from wedge plate, see Figure 1c) to capture circumferential strain signals. Also, six ESGs, called AT1-3 and AT6-8, were positioned at the near-top anchor head (9 mm from wedge plate, see Figure 1c) to capture axial strain signals. For the near-bottom anchor head, six ESGs, called CB1-3 and CB6-8, were positioned at the near-bottom anchor head (5 mm from the bearing plate) to capture circumferential strain signals. Also, six ESGs, called AB1-3 and AB6-8, were positioned at the near-bottom anchor head (10 mm from the wedge plate) to capture axial strain signals. Figure 1d shows the real

view of ESGs on the anchor head in the axial and circumferential directions.

The distribution of strain variation within a region of prestressing strand was also examined, as shown in Figure 2. For the 9-strand anchorage system with a center strand 9, the surface area on the anchor head surface was about 60 × 65 mm, in which 60 mm is the width along with the circumference, and the other is the height from the bearing plate to top anchor surface (see Figure 1c). Totally, 25 ESGs divided into five layers with 5 ESGs for each layer were used to capture signals on the surface of Strand 7. The ESGs were namely CT7-1 ~ CT7-5 (layer close to wedge plate), CT7-6 ~ CT7-10, CT7-11 ~ CT7-15 (middle of the anchor head), CT7-16 ~ CT7-20, and CT7-21 ~ CT7-25 (close to bearing plate). Figure 2b illustrates the real view of ESGs placed surrounding Strand 7 for measuring anchorage responses under PS force loss.

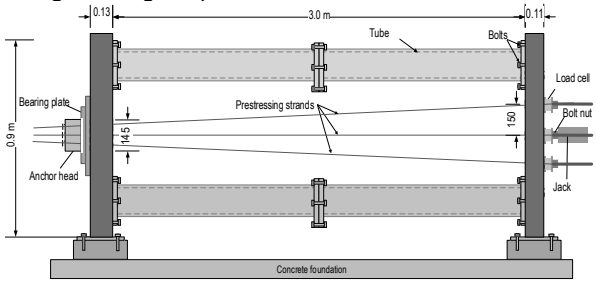

a) Overview setup of anchorage zone on supported frame

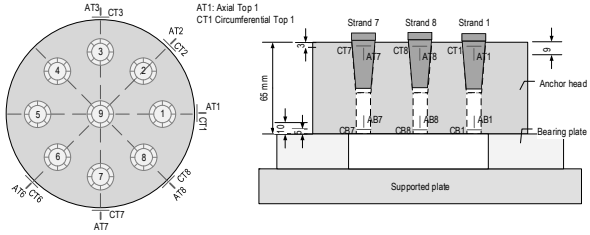

b) ESGs on top-view *c) ESGs on side-view*

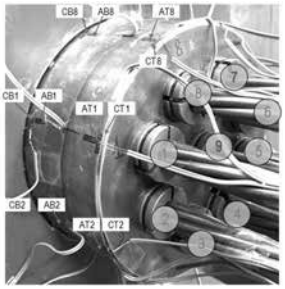

d) Real view of ESGs on the anchor head

Figure 1 Experimental setup of ESGs for strain responses measurement

2.3 Instrumentation for strain measurement

The signal conditioner consists of TML SB 120B (bridge boxes), a data recorder KYOWA, and DCS-100A software installed on the PC. The data recorder with a sampling frequency of 1 Hz to 10 kHz is operated by software DSC-100A (data analysis). It includes low/high pass filters for filtering noises during measurement. The sampling frequency was set as 1 Hz with a duration set as 25 seconds.

The strain change of a monitored structure is proportional to the variation of resistance wire (foil) in ESGs [18]. The resistance change is very small, and it requires a Wheatstone bridge circuit to convert it to the voltage output. For the experimental instrumentation, the EDX-100A system can catch the change of ESG of 0.1με.

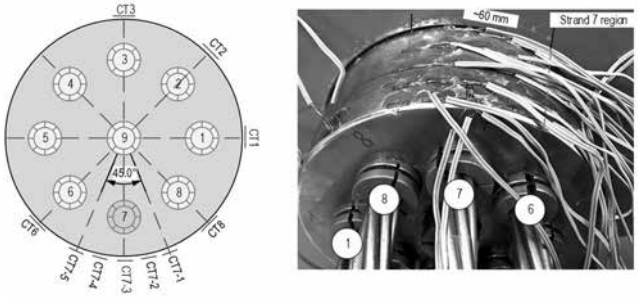

a) ESGs on top-view *b) Real view of ESGs surrounding Strand 7*

Figure 2 Deployment of ESGs along with circumferential direction

2.4 Test procedures and scenarios

Six test cases, namely PS1-PS6, were designed to measure the anchorage's responses, as listed in Table 1. The procedures were briefly described as follows. At first, each of the nine strands was pre-stressed with an average tension of approximately 14.12 tons to simulate the intact case of the structure (i.e., PS1). Second, the force of Strand 7 was decreased to 7 tons, while forces in the other strands were kept almost constant values to simulate the prestress loss (PS) in PS2. Third, to simulate the next intact case (PS3), Strand 7 was stressed to approximately 14 tons. For, a force of Strand 9 was steadily decreased to 7.0 tons while the other strands were maintained near-constant values (14.13 tons) to simulate the loss of the center strand in PS4. Five, to simulate the intact state (PS5), Strand 9 was re-stressed with the average force of 14.0 tons. Last, the force of Strand 7 was reduced to 7.0 tons to simulate prestress loss of Strand 7 in PS6. Due to the symmetry of the tested structure, strain responses measured at Strands 4-5 were assumed to have the same values as those at Strands 2 and 1.

For the prestress loss PS1-PS4, the strain signals of ESGs along with circumferences at the near-top and near-bottom anchor head were recorded, as noted in Table 1. After measuring strain signals in these tests, some ESGs were removed to install ESGs (CT7-1 ~ CT7-25) within the region of Strand 7. For the prestress loss PS5-PS6, the strain signals of CT7-1 ~ CT7-25 were recorded.

Table 1 Prestressing scenarios for strain responses measurement

Case	Prestress force	Measurement of ESGs
PS1	All strands: pre-stressed about 14.12 tons	CT1-CT3, CT6-CT8 CB1-CB3, CB6-CB8 AT1-AT3, AT6-AT8 AB1-AB3, AB6-AB8
PS2	Strand 7: 7 tons, others: about 14.13 tons	
PS3	All strands: pre-stressed about 14.11 tons	
PS4	Strand 9: 7 tons, others: about 14.13 tons	
PS5	All strands: pre-stressed about 14.0 tons	CT7-1 ~ CT7-25
PS6	Strand 7: 7 tons, others: about 14.12 tons	

3. ANALYSIS OF STRAIN RESPONSES OF ANCHORAGE UNDER PRESTRESS LOSS

3.1 Experimental strain responses

Figure 3a-b shows the strain responses obtained from CT 7 (circumferential strain at near-top) and AT7 (axial strain at near-top) under the prestress force loss of Strand 7 in PS1-PS2. As presented in Figure 1b, the CT7 and AT7 were positioned close to Strand 7. The variation of circumferential strain was more significant than that of the axial strain.

Figure 4a-b shows the strain responses obtained from CB 7 (circumferential strain at near-bottom) and AB7 (axial strain at near-top) under the prestress force loss of Strand 7 in PS1-PS2. As observed, the variation of axial strain was more significant than that of the circumferential strain. This observation is opposite to the strain responses measured at the near-top anchor head.

Moreover, the variation in strain signals of CT 7 (Figure 3b) was about three times higher than that of CB7 (Figure 4b). Meanwhile, the variation in strain signals of AB 7 was about 17 times larger than that of AT7.

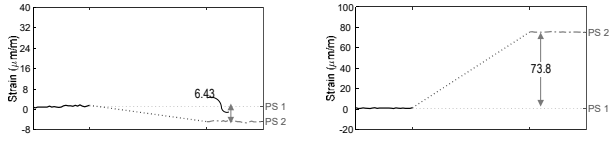

a) AT7: axial direction *b) CT7: Circumferential direction*

Figure 3 Time-history of near-top ESGs under PS loss of Strand 7

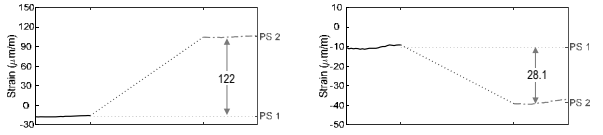

a) AB7: axial direction *b) CB7: Circumferential direction*

Figure 4 Time-history of near-bot ESGs under PS loss of Strand 7

3.2 Strain variation induced by prestress loss

The variations of strain components in the anchorage system for the near-top and near bottom anchor head was plotted over the anchor's section, as shown in Figure 5-6. For strain variation at the near-top anchor head, the prestress loss of the outer strand (Strand 7) led to major changes in the strain components at the location close to this strand, while the force loss of the center strand produced almost the uniform strain changes on circumferences of the anchor head. Notably, the circumferential strain variation at Strand 7 was positive (tension), while the axial one at Strand 7 was negative (compression). Moreover, the magnitude of circumferential strain variation (Figure 5b) was about five times larger than that of the axial strain (Figure 5a).

For strain variation at the near-bottom anchor head, the prestress loss of the outer strand (Strand 7) also led to major changes in the strain components at the location close to Strand 7, and the force loss of the center strand produced almost the uniform strain changes on circumferences of the anchor head. Moreover, the circumferential strain variation at Strand 7 was negative (compression), but the axial one at Strand 7 was positive (tension). The magnitude of axial strain variation (Figure 6a) was more significant than that of the circumferential one (Figure 6b).

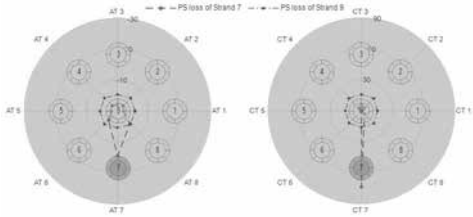

a) Axial strain variation *b) Circumferential strain variation*

Figure 5 Variations of strain components (μmm/mm) measured at near-top anchor head under PS loss of Strand 7 and Strand 9.

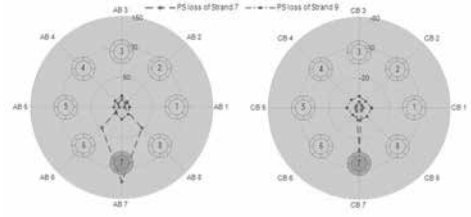

a) Axial strain variation *b) Circumferential strain variation*

Figure 6 Variations of strain components (μmm/mm) measured at near-bottom anchor head under PS loss of Strand 7 and Strand 9.

Comparing strain responses for the two positions, the near bottom anchor exhibits more changes in axial strain compared to the one in circumferential at the top. However, the circumferential strain mostly changed at the location close to damaged strands. Meanwhile, the axial strain also causes changes at adjunct strands (i.e., Strands 6&8). Thus, the circumferential strain is the potential to be used for strand monitoring.

Figure 7 shows circumferential strain variation within the anchor head's surface of Strand 7 under PS loss of Strand 7. As seen in the figure, the strain change was nonlinear in two directions. The maximum tension-strain value occurs at the near-top anchor head, and it reduces and gets a negative value at the near-bottom (see Figure 7). Moreover, Figure 7b illustrates the strain distribution on the cross section of the near-top anchor head. It is observed that maximum strain change at CT7-3 (closest distance to the Strand 7), and the strain value was abruptly changed within the region of this strand. The strain changes at adjunct strands can be ignored.

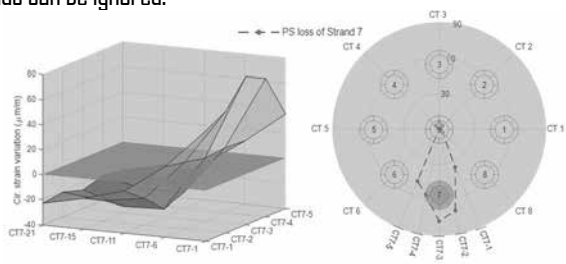

a) Strain changes on anchor's surface at Strand 7 *b) Strain changes at near-top anchor*

Figure 7 Variations of circumferential strain (μmm/mm) under PS loss of Strand 7

3.3 Estimation of prestress loss using strain change

Since the circumferential strain reaches the highest value at the damaged strand and zeroes at the other strands, this strain component is potentially used for prestress loss estimation. At first, the empirical relationship between prestressing loss and strain variation was built for an outer strand and the center strand. Then, the strain changes at other strands can be input into the equation to estimate prestress force loss.

To build empirical equation, prestress loss was performed on an outer strand (Strand 8) and a center strand (Strand 9). For each PS loss of strand, the prestress force was reduced from 14.0 tons to zero with five loading steps, while forces of the other strand were kept near-constant (about 14 tons). Circumferential strain signals were measured at near-top CT8 for two cases.

As shown in Figure 8, the relationship between $\Delta\varepsilon$ (circumferential strain change) and ΔP was analyzed for CT 8. The variations of strain were almost linearly increased with respect to ΔP. In addition, the damaged outer strand caused more variations in strain components than those of the center strand. Empirical equations were built, as shown in the figures.

By substituting circumferential change at Strand 7 under the breakage of Strand 7 (i.e., 73.8 μmm/mm, see Figure 3b) into equation PSL1 (see Figure 8a), prestress loss was predicted as 6.62 tons). Similarly, substituting circumferential change at Strand 7 under the breakage of Strand 9 (i.e., 15.77 μmm/mm, see Figure 5b) into equation PSL2 (see Figure 8b), prestress loss was predicted as 7.49 tons). The prestress loss prediction was about six percent different compared to the inflicted ones.

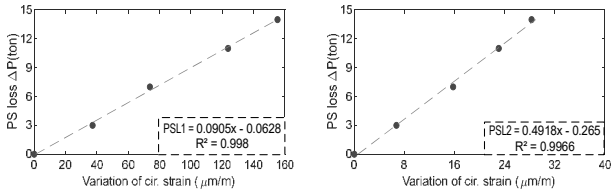

a) CT8 under PS loss of Strand 8 *b) CT8 under PS loss of Strand 9*

Figure 8 Relationship between prestress loss-strain variation for outer-center strands

4. CONCLUDING REMARKS

This study presented the experimental results on strain responses of the un-bonded post-tensioning anchorage system. First, the arrays of ESGs were mounted on the anchor head to capture strain changes under a series of simulated prestress force losses. Then, strain variations were utilized to determine strain components sensitive to prestress force losses. Last, the empirical equations between force loss and strain changes were conducted for prestress loss estimation.

From the experimental result, it can be concluded. First, the circumferential strain variation got the highest value at the near-top anchor head and close to the damaged strand. Second, the axial strain got a high value at the near-bottom anchor in regions close to damaged strands. Last, prestress force loss is promising to be estimated using the proposed empirical equations.

Further works need to be considered: (1) strain responses of the anti-symmetric anchorage systems and (2) effects of concrete block on the strain responses in prestressed concrete structures.

REFERENCES

1. Tadros, M.K., Omaishin, N.A., Seguirant, S.J., and Gallt, J.G. (2003), *Prestress losses in pretensioned high-strength concrete bridge girders*. Transportation Research Board.

2. Goldsberry, B. (2013) *Post-Tensioning Best Practice Update and New Directions for Post-Tensioned Structures*.

3. Mehrabi, A.B., Ligozio, C.A., Ciolko, A.T., and Wyatt, S.T. (2010), "Evaluation, rehabilitation planning, and stay-cable replacement design for the hale boggs bridge in Luling, Louisiana," *Journal of Bridge Engineering*, vol. 15(4), pp. 364-372.

4. Hiba, A.J., and Glisic, B. (2018), "Monitoring of long-term prestress losses in prestressed concrete structures using fiber optic sensors," *Structural Health Monitoring*, vol. 18(1), pp. 254-269.

5. James, G., Pianigiani, G., White, J., and Patanjali, K. (2018) *Genoa bridge collapse: the road to tragedy*.

6. Ho, D.D., Kim, J.T., Stubbs, N., and Park, W.S. (2012), "Prestress-force estimation in PSC girder using modal parameters and system identification," *Advances in Structural Engineering*, vol. 15(6), pp. 997-1012.

7. Kim, J.T., Park, J.H., Hong, D.S., and Park, W.S. (2010), "Hybrid health monitoring of prestressed concrete girder bridges by sequential vibration-impedance approaches," *Engineering Structures*, vol. 32(1), pp. 115-128.

8. Hamed, E., and Frostig, Y. (2006), "Natural frequencies of bonded and unbonded prestressed beams–prestress force effects," *Journal of Sound and Vibration*, vol. 295(1-2), pp. 28-39.

9. Law, S.S., and Lu, Z.R. (2005), "Time domain responses of a prestressed beam and prestress identification," *Journal of Sound and Vibration*, vol. 288(4-5), pp. 1011-1025.

10. Dang, N.L., Huynh, T.C., and Kim, J.T. (2019), "Local strand-breakage detection in multi-strand anchorage system using an impedance-based stress monitoring method-feasibility study," *Sensors (Basel)*, vol. 19(5).

11. Ai, D., Luo, H., and Zhu, H. (2019), "Numerical and experimental investigation of flexural performance on pre-stressed concrete structures using electromechanical admittance," *Mechanical Systems and Signal Processing*, vol. 128, pp. 244-265.

12. Pham, Q.Q., Dang, N.L., and Kim, J.T. (2021), "Piezoelectric Sensor-Embedded Smart Rock for Damage Monitoring in a Prestressed Anchorage Zone," *Sensors*, vol. 21(2).

13. Na, W.S. (2018), "Low cost technique for detecting adhesive debonding damage of glass epoxy composite plate using an impedance based non-destructive testing method," *Composite Structures*, vol. 189, pp. 99-106.

14. Na, W.S. (2017), "Distinguishing crack damage from debonding damage of glass fiber reinforced polymer plate using a piezoelectric transducer based nondestructive testing method," *Composite Structures*, vol. 159, pp. 517-527.

15. Ai, D., Lin, C., Luo, H., and Zhu, H. (2020), "Temperature effect on electromechanical admittance–based concrete structural health monitoring_LOI," *Structural Health Monitoring*, vol. 19(3), pp. 661-692.

16. Abdullah, A.B.M., Rice, J.A., and Hamilton, H.R. (2015), "Wire breakage detection using relative strain variation in unbonded posttensioning anchors," *Journal of Bridge Engineering*, vol. 20(1), pp. 1-12.

17. Lan, C., Zhou, Z., and Ou, J. (2014), "Monitoring of structural prestress loss in RC beams by inner distributed Brillouin and fiber Bragg grating sensors on a single optical fiber," *Structural Control and Health Monitoring*, vol. 21(3), pp. 317-330.

18. Tml, TML precise & flexible strain gauges, Tokyo Sokki Kenkyujo Co., L., https://www.bestech.com.au/wp-content/uploads/brochures/Cat_-_STRAIN_GAUGES_-_TML.pdf, Accessed on, Jan 2019.